Intermodal interference of LP_{01} and LP_{11} modes in panda fibers

Feng Liu (刘 丰)*, Delan Cao (曹德兰), Xuan Guo (郭 璇), and Xin Lu (芦 鑫)

College of Information Science and Engineering, Yanshan University, Qinhuangdao 066004, China

**Corresponding author: kennan@ysu.edu.cn*

Received October 24, 2011; accepted December 28, 2011; posted online February 24, 2012

LP_{01} and LP_{11} mode interferences in high-birefringence (Hi-Bi) panda fibers are theoretically and experimentally presented. The propagation characteristics of both the fundamental and second-order modes in Hi-Bi panda fibers are investigated, and the interference output intensity distribution of the LP_{01} and LP_{11} modes in panda fibers are thoroughly examined. An experiment is conducted to verify the feasibility of modal interference sensors. The results show that the two-lobe interference pattern of panda fibers generates energy exchanges when external strain is applied on the fiber. Moreover, Hi-Bi panda fibers can be used to design voltage sensors.

OCIS codes: 060.2310, 030.4070, 060.2370.

doi: 10.3788/COL201210.060602.

Fiber-optic sensors based on the intermodal interference technology of polarization-maintaining optical fibers have been successfully demonstrated in the past few years[1−3]. Based on this technology, a number of physical quantities, such as strain, temperature, voltage, liquid, hydrocarbon, etc., can be measured[4−7]. However, published reports on intermodal interference technology usually concentrate on elliptical-core fibers and photonic crystal fibers[8−11]. Recently, we have adopted the intermodal interference in panda fibers in sensing applications. In previous reports, the intermodal interference characteristics of panda fibers have not been thoroughly analyzed, and the analysis of panda fibers are mainly concerned on the influence of stress region area and position on stress-induced birefringence[12].

In this letter, the intermodal interference of LP_{01} and LP_{11} modes in panda fibers is investigated and adopted to the design of fiber-optic sensors. The mode propagation characteristics are calculated, and the interference output intensity patterns in the panda fibers are illustrated. Furthermore, an experiment is conducted to demonstrate the intermodal interference. The theoretical and experimental results are useful in designing fiber-optic sensors composed of panda fibers based on intermodal interference.

As in previous works, the difference in the propagation constants of individual modes causes intermodal interference[13]. For panda fibers, the propagation constants of modes can be expressed as[14]

$$\beta_{mn} = k_0\sqrt{n_1^2 - \frac{U_{mn}^2(V)}{V^2}(n_1^2 - n_2^2)}, \tag{1}$$

where β_{mn} is the propagation constant of the LP_{mn} mode, $k_0 = 2\pi/\lambda$, λ is the wavelength in the vacuum, and n_1 and n_2 are the refractive indexes of the core and cladding, respectively. Moreover, V is the normalized frequency defined by $V = k_0 a\sqrt{n_1^2 - n_2^2}$, whereas a is the semi-diameter of the fiber core.

The transverse vectors of the electric ($\mathbf{E}$) and magnetic ($\mathbf{H}$) fields of an optical fiber can be expressed as the sum of modes

$$\begin{bmatrix} \mathbf{E} \\ \mathbf{H} \end{bmatrix}(x,y,z,t) = \sum_{j=1}^{n} a_j \begin{bmatrix} \mathbf{e}_j \\ \mathbf{h}_j \end{bmatrix}(x,y) \cdot \exp[-\mathrm{i}(\omega t + \beta_j z)], \tag{2}$$

where a_j is the amplitude of the jth mode, $\mathbf{e}_j$ and $\mathbf{h}_j$ are the functions that describe the jth mode field distribution, ω is the angular frequency, t is the time, z is the coordinate along which the modes propagate, x and y are the coordinates perpendicular to z, and β_j denotes the propagation constants of the jth mode.

For a linearly birefringent weakly guiding optical fiber, the LP_{01} and LP_{11} modes' electric field can be considered as a superposition of the electric fields $\mathbf{E}_{01}$ and $\mathbf{E}_{11}$ of each mode[15]

$$\mathbf{E}(r,\varphi,z) = \xi_0\mathbf{E}_{01}(r,\varphi,z) + \xi_1\mathbf{E}_{11}(r,\varphi,z), \tag{3}$$

where ξ_0 and ξ_1 are the mode excitation coefficients confined by the function $\xi_0^2 + \xi_1^2 = 1$. Assuming that no external perturbations lead to power coupling between the LP_{01} and LP_{11} modes, the electric field of each mode can be expressed as

$$\mathbf{E}_{01}(r,z) = A_1(z)f_{01}(r)\mathbf{x} + A_2(z)f_{01}(r)\mathbf{y}, \tag{4}$$

$$\begin{aligned}\mathbf{E}_{11}(r,\varphi,z) =& B_1(z)f_{11}^{\mathrm{e}}(r,\varphi)\mathbf{x} + B_2(z)f_{11}^{\mathrm{o}}(r,\varphi)\mathbf{x} \\ &+ B_3(z)f_{11}^{\mathrm{e}}(r,\varphi)\mathbf{y} + B_4(z)f_{11}^{\mathrm{o}}(r,\varphi)\mathbf{y},\end{aligned} \tag{5}$$

where $f_{01}(r)$, $f_{11}^{\mathrm{e}}(r,\varphi)$, and $f_{11}^{\mathrm{o}}(r,\varphi)$ are the spatial distribution functions of the LP_{01}, LP_{11}^{e}, and LP_{11}^{o} modes ("e" for even and "o" for odd), respectively, $A_i(z)$ and $B_i(z)$ are the amplitude coefficients of the corresponding polarization modes, and $\mathbf{x}$ and $\mathbf{y}$ are the unit vectors along the fiber section. Assuming that only the LP_{01}^{y} and $LP_{11}^{y;\mathrm{e}}$ modes can be excited and sustained in the panda fiber, the electric field can be simplified as

$$\mathbf{E}(r,\varphi,z) = \xi_0'\mathbf{E}_{\mathrm{LP}_{01}}(r,\varphi,z)\mathbf{y} + \xi_1'\mathbf{E}_{\mathrm{LP}_{11}^{\mathrm{e}}}(r,\varphi,z)\mathbf{y}. \tag{6}$$

The y-oriented interference output light intensity of the LP_{01}^{y} and $\mathrm{LP}_{11}^{y,\mathrm{e}}$ modes can be expressed as

$$\begin{aligned} I(r,\varphi,z) &= |\mathbf{E}(r,\varphi,z)|^2 \\ &= |\mathbf{E}_{\mathrm{LP}_{01}}(r,\varphi,z)\mathbf{y} + \mathbf{E}_{\mathrm{LP}_{11}^{\mathrm{e}}}(r,\varphi,z)\mathbf{y}|^2 \\ &= \mathbf{E}_{\mathrm{LP}_{01}}(r,\varphi,z)^2\mathbf{y} + \mathbf{E}_{\mathrm{LP}_{11}^{\mathrm{e}}}(r,\varphi,z)^2\mathbf{y} \\ &\quad + 2\mathbf{E}_{\mathrm{LP}_{01}}(r,\varphi,z)\mathbf{E}_{\mathrm{LP}_{11}^{\mathrm{e}}}(r,\varphi,z)\cos(\Delta\phi)\mathbf{y}, \end{aligned} \tag{7}$$

where $\Delta\phi = \Delta\beta\Delta l$ is the phase difference between the LP_{01}^{y} and $\mathrm{LP}_{11}^{y,\mathrm{e}}$ modes. Equation (7) indicates that the output light intensity varied considerably with $\Delta\phi$. Figure 1 illustrates the intensity patterns for $\Delta\phi$ changing from 0 to 2π.

The simulation results show that the interference output light intensity distribution has an oscillatory two-lobe pattern. As the phase difference $\Delta\phi$ changes from 0 to $\frac{\pi}{2}$, the interference energy will transfer from the left to the right lobe. Once the phase difference reaches $\frac{\pi}{2}$, the energy will be equally distributed in the two lobes. When the phase difference continues to change from $\frac{\pi}{2}$ to π, the energy will transfer totally from the left to the right lobe. Thus, the output interference light intensity realizes energy exchange from the left to the right lobe when the phase difference shifts from 0 to π. Moreover, the two-lobe oscillation pattern is still manifested when the phase difference shifts from π to 2π.

In this case, if the intensity of one or two lobes is monitored, the phase difference can be obtained and the phase difference shift caused by external disturbance can be measured.

The propagation character and wavelength for the dual-mode operation in panda fibers are determined by adapting the finite-element analysis in the simulation. An ideal panda fiber with no geometrical imperfections in its cladding and no perturbations is considered in this study, and its cross section is illustrated in Fig. 2.

The core and cladding refractive indexes are $n_1 = 1.464$ and $n_2 = 1.45$, respectively. The cladding material is pure SiO_2. The core is Ge-doped, whereas the stress region is Bo-doped. The photoelastic coefficients are $c_1 = 0.7572448\times10^{-12}$ m^2/N and $c_2 = 4.18775\times10^{-12}$ m^2/N. The fiber's Young's modulus ratio is $E = 78\times10^9$ m^2/N, and the Poisson's ratio is $\nu = 0.186$. The thermal expansions of the core, cladding, and stress regions are $\alpha_1 = 22.15\times10^{-7}$ /°C, $\alpha_2 = 5.4\times10^{-7}$ /°C, and $\alpha_3 = 14.5\times10^{-7}$ /°C, respectively. The geometrical parameters of the panda fiber are $a = 2$ μm, $b = 62.5$ μm, and $r = 7.5$ μm, and the stress applying radius is $l = 16.5$ μm.

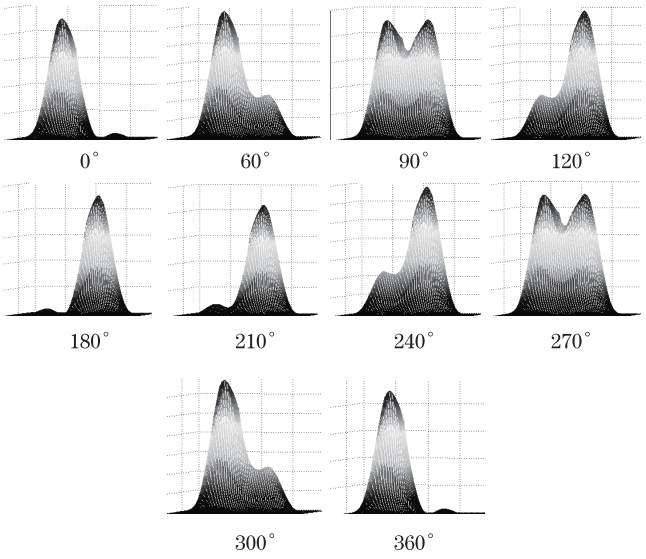

Fig. 1. Distributions of output interference light intensity at the phase position of 0—2π in a panda fiber.

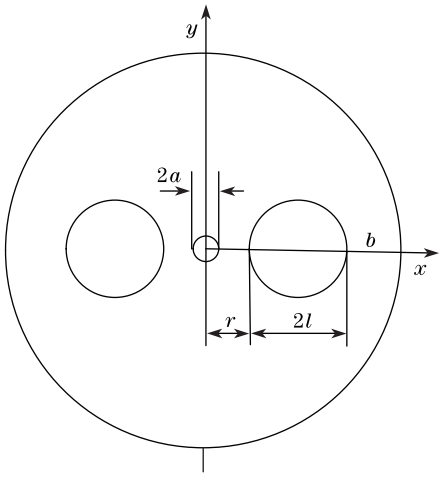

Fig. 2. Cross-sectional structure of the panda fiber.

The operation wavelength should be carefully chosen in adapting the modular interference theory in fiber-optic sensors. Thus, the relationship between the normalized frequency V and the effective index β/k_0 of each mode was determined to investigate the suitable operation wavelength, and the result is shown in Fig. 3. The curve indicates that more modes are propagated in the panda fiber as the normalized frequency increases. However, when the normalized frequency $V = \frac{2\pi a}{\lambda}\sqrt{n_1^2 - n_2^2}$ is between 2.73 and 4.02, only the LP_{01} and LP_{11} modes can be propagated in the fiber. It indicates that the practicable wavelength is between 929.7 and 629.8 nm. Here, the $\mathrm{LP}_{11}^{y,\mathrm{o}}$ and $\mathrm{LP}_{11}^{y,\mathrm{e}}$ modes seem to be excited at the same time in Fig. 3. However, the real situation is that, when a plant-wave is focused in the fiber core, the amplitude coefficient of all odd modes are zero[13]. Thus, only the LP_{01} and high-order even modes can be excited in the panda fiber. Furthermore, although the panda fiber cannot separate the even and odd modes spontaneously with the asymmetric fiber structure as in an elliptical-core fiber[3], the same dual-mode transmission can be achieved.

In eliminating the modes in the x orientation, a polarizer is needed to select the y orientation polarization modes (LP_{01}^{y} and $\mathrm{LP}_{11}^{y,\mathrm{e}}$).

The intermodal interference beat length is an important parameter for designing intermodal interference sensors as it decides the range of external disturbance that can be measured. The intermodal interference beat length can be defined as $L_{\mathrm{M}} = \frac{k_0}{\Delta\beta} = \frac{k_0}{\beta_{\mathrm{LP}_{01}} - \beta_{\mathrm{LP}_{11}}}$. Then, the relationship between L_{M} and normalized frequency can be calculated, and the results are shown in Fig. 4.

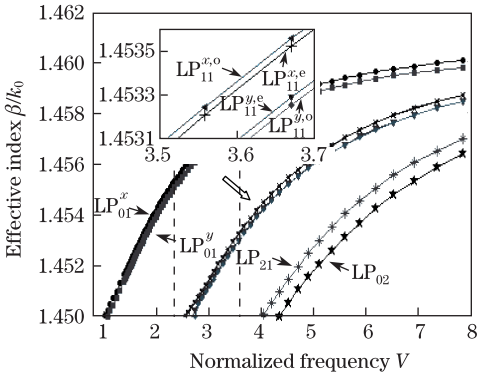

Fig. 3. Relationships between several modes and the normalized frequency V.

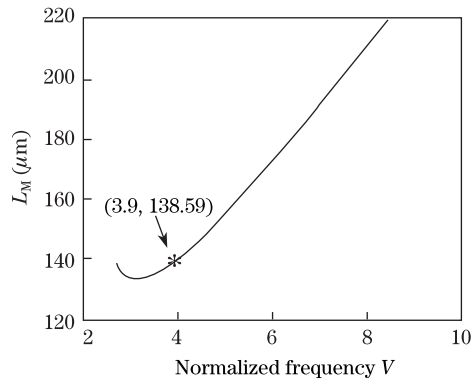

Fig. 4. Relationship between $L_{\rm M}$ and the normalized frequency V.

Figure 4 indicates that $L_{\rm M}$ will increase according to the normalized frequency increase. In particular, when the normalized frequency is 3.9, the wavelength is 650 nm, and $L_{\rm M}$ is 138.59 μm.

An experiment was conducted to verify the feasibility of modular interference sensors based on panda fibers (Fig. 5).

In Fig. 5, the light from the 650-nm laser source is polarized using a fiber polarizer and then led into a piece of panda fiber. The panda fiber is wrapped with a $PbZrTiO_3$ (PZT) tube, whose driver voltage can be adjusted manually. The output end of the panda fiber is fixed on a three dimensional (3D) adjustable fiber holder. Then, the modular phase difference can be adjusted by the voltage applied on the PZT. The two output lobes from the panda fiber is picked up with two pin holes on a screen and is then aimed on two positive–intrinsic–negative photodiodes, as shown in Fig. 5. Moreover, the output current from the two photodiodes is amplified and processed in the signal process unit, where we realize "difference divided by sum" (that is, $U_{\rm o} = K\frac{I_1-I_2}{I_1+I_2}$, where $U_{\rm o}$ is the output voltage of the experimental system, K is a coefficient, and I_1 and I_2 denote the two output lobes' intensities, respectively.)

If we replace the pin-hole screen with a screen without holes, the output lobe oscillation can be observed as shown in Fig. 6 when the direct current (DC) voltage of the PZT is adjusted.

Figure 6(a) shows that the left lobe's intensity is larger than that of the right lobe, whereas Fig. 6(b) shows that the left and right lobes have equal intensities. Figure 6(c) indicates that the left lobe's intensity is smaller than that of the right lobe.

For the experiment shown in Fig. 5, the parameters of the PZT tube are as follows: the outer diameter $r = 40$ mm, the thickness $d = 3.2$ mm, the piezoelectric coefficient $d_{\rm z} = 200 \times 10^{-12}$ m/V, and the panda fiber wrapped on the PZT has $N = 70$ turns. According to the converse piezoelectric effect, the elongation of the panda fiber caused by the applied voltage on PZT can be expressed as

$$\Delta L = \pi r d_{\rm z} \frac{\Delta U_{\rm PZT}}{d} N, \tag{8}$$

where $\Delta U_{\rm PZT}$ is the variable voltage applied on the PZT. From Eq. (8), the intermodal interference beat length can be calculated when the two output lobes complete a periodic energy exchange. In the experiment, when the DC voltage is adjusted from 35 to 145 V, the two output lobes' intensities will change from one equal status to another, which is a half period. Thus, when the $\Delta U_{\rm PZT} = 110$ V is substituted into Eq. (8), $\frac{1}{2}\Delta L \cong 60.5$ μm can be obtained, and the beat length is about 121 μm. The comparison between the experimental and theoretical results shows that although they do not coincide very well, the modular interference beat length is still more than 100 μm. The possible reasons causing this error are the asymmetrical wrapping strain and radial stress of the panda fiber.

Furthermore, a 50-Hz sinusoidal alternating current (AC) voltage is applied on the PZT to demonstrate the feasibility of the sensors designed using the panda fiber modular interference method. However, it must be mentioned that, to achieve novel response characteristics, the DC voltage must be carefully adjusted to ensure that the two output lobes' intensities are as equal as possible before the AC voltage is applied. Figure 7 shows the oscillograph result of the experimental system's output.

Figure 7 shows that when the two lobes' intensities are equal before the AC voltage is applied on the PZT,

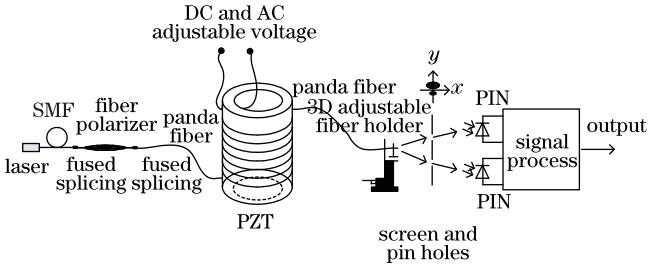

Fig. 5. Experimental setup for investigating the feasibility of modular interference sensors.

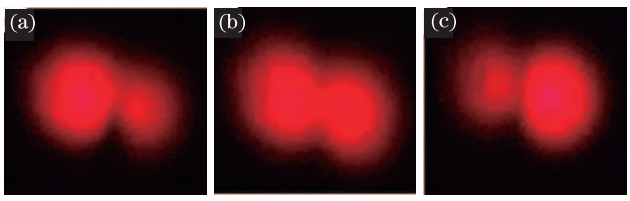

Fig. 6. Two-lobe oscillation results of the intermodal interference in a panda fiber. The left lobe's intensities are (a) larger, (b) equal, and (c) smaller than those of the right lobe.

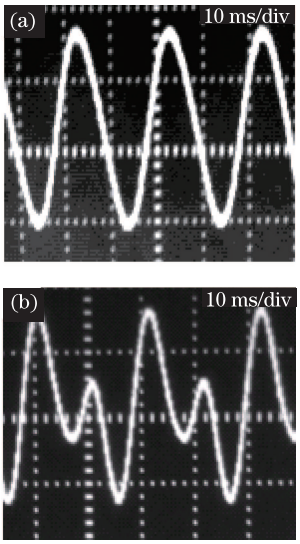

Fig. 7. Oscillograph result after the AC voltage is applied to the PZT. The two lobes' intensities are (a) equal and (b) unequal before the AC voltage is applied.

the sensor system shown in Fig. 6 can reflect the AC voltage very well as in Fig. 7(a). Meanwhile, Fig. 7(b) shows that when the two lobes' intensities are not equal after the DC voltage adjustment, the oscillograph result becomes distorted. Thus, an appropriate quiescent point must be set to guarantee that the modular interference sensors are working well.

In conclusion, the intermodal interference characteristics of the high-birefringence (Hi-Bi) panda fiber are thoroughly analyzed, and an experiment demonstrates the feasibility of designing optical-fiber sensors based on the modular interference in panda fibers. The theoretical calculation and experimental results indicate that the two modular interference output lobes' intensities exchange energy when external strain is applied on the panda fiber. Afterward, a sensor system for measuring AC voltage is established. The results show that intermodal interference in panda fibers is a novel technique for fabricating fiber-optic sensors. Furthermore, other interesting applications, such as the measurement of strain, temperature, high voltage, pressure, etc., can be actualized using the panda fiber's modular interference.

This work was supported by the National Natural Science Foundation of China (No. 60907033) and Hebei Natural Science Foundation of China (No. E2009000373).

References

1. K. A. Murphy, M. S. Miller, A. M. Vengsarkar, and R. O. Claus, J. Lightwave Technol. **8,** 1688 (1990).
2. A. Kumar, N. K. Goel, and R. K. Varshney, J. Lightwave Technol. **19,** 358 (2001).
3. K. Bohnert, P. Gabus, J. Kostovic, and H. Brandle, Opt. Laser Eng. **43,** 511 (2005).
4. K. Bohnert, G. C. de Wit, and J. Nehring, J. Lightwave Technol. **13,** 94 (1995).
5. I. Martincek, D. Pudis, D. Kacik, and K. Schuster, Optik **122,** 707 (2011).
6. Y. Wu, X. Deng, and X. Zhuang, Sens. Actuator B **122,** 127 (2007).
7. R. P. McCue, J. E. Walsh, F. Walsh, and F. Regan, Sens. Actuator B **114,** 438 (2006).
8. F. Liu, W. Bi, and X. Guo, Acta Opt. Sin. (in Chinese) **29,** 219 (2009).
9. X. Lu, W. Bi, S. Ma, and F. Liu, Chinese J. Lasers (in Chinese) **38,** 1105003 (2011).
10. W. Chen, S. Lou, L. Wang, and S. Jian, Chin. Opt. Lett. **8,** 986 (2010).
11. D. Kácik, I. Turek, I. Martincek, J. Canning, N. A. Issa, and K. Lyytikäinen, Opt. Express **12,** 3465 (2004).
12. P. Kniazewski, T. Kozacki, and M. Kujawinska, Opt. Laser Eng. **47,** 259 (2009).
13. A. Safaai-Jazi and J. C. McKeeman, J. Lightwave Technol. **9,** 1047 (1991).
14. I. Martincek and D. Pudis, Optik **121,** 1660 (2010).
15. T. A. Eftimov and W. J. Bock, J. Lightwave Technol. **11,** 1925 (1993).